Spin solitons and spin waves in chiral and racemic molecular based ferrimagnets

R. Morgunov,[1,2] M. V. Kirman,[1] K. Inoue,[2] Y. Tanimoto,[2] J. Kishine,[3] A. S. Ovchinnikov,[4] and O. Kazakova[5]
[1]*Institute of Problems of Chemical Physics, Chernogolovka, 142432, Russia*
[2]*Graduate School of Science, Hiroshima University, Higashi-Hiroshima 739-8526, Japan*
[3]*Graduate School of Engineering, Kyushu Institute of Technology, Otbata, Kitakyushu 804-8550, Japan*
[4]*Department of Physics, Ural State University, 620083 Ekaterinburg, Russia*
[5]*National Physical Laboratory, Teddington, TW 11 OLW, United Kingdom*
(Received 20 September 2007; revised manuscript received 4 March 2008; published 15 May 2008)

Resonant modes corresponding to a spin-soliton resonance (SSR) and a spin-wave resonance (SWR) have been detected and distinguished in the spectra of the electron spin resonance (ESR) of two-dimensional $[Cr(CN)_6][Mn(S)\text{-}pnH\text{-}(H_2O)]H_2O$ [green needle (GN)] chiral single crystals and three-dimensional $[Mn\{(R/S)\text{-}pn\}]_2$ $[Mn\{(R/S)\text{-}pn\}_2(H_2O)][Cr(CN)_6]_2$ [yellow needle (YN)] single crystals. The spin-soliton resonance has been detected in the ESR spectrum of the chiral YN crystals and has not been observed in the spectra of the racemic GN crystals. This is a direct experimental evidence that the collective spin excitations in molecular magnetic crystals depend on the crystal chirality. The temperature and the angular dependences of the effective exchange constants obtained from the ESR spectra are in good agreement with the experimental data received by means of a superconducting quantum interference device magnetometry. The temperature dependencies of the magnetic susceptibilities corresponding to the integral intensities of the resonance lines are different for the SSR and the SWR contributions to the ESR spectrum. It enables us to distinguish the nature of the resonant lines in the intermixture of two sequences of the resonance lines, which have been measured for arbitrary orientations of the static external magnetic field.

DOI: 10.1103/PhysRevB.77.184419 PACS number(s): 75.50.Xx, 75.30.Fv

I. INTRODUCTION

Spin waves and spin-density solitons were discovered in thin ferromagnetic films, and a large amount of experimental and theoretical research has been dedicated to this exciting area.[1–4] Recently, the interest in spin-wave phenomena has revived again as theoretical predictions of new types of magnetic spin excitations in nanostructures[5,6] and molecular based magnets[7,8] were reported. By manipulating the chemical design in these new magnetic materials, it is possible to construct novel electron and magnetic structures, as well as alter exchange interactions and magnetic anisotropies. This precise chemical and material tailoring provides a chance to obtain novel fundamental information about the nature of spin waves and other collective spin excitations. One of the most important examples of such a chemical design is chiral molecular based magnets. Presently, a large number of metal-organic compounds without an inversion symmetry and a remarkable contribution of the Dzyaloshinskii–Moriya (DM) exchange interaction to the magnetic properties have been synthesized.[9–15] For some of these compounds, the structural chirality induces the chirality of the spin density, as revealed by neutron and muon diffractions.[15] The interplay between the structural chirality and the spin density is usually explained by spin-orbital interactions and the anisotropy field in ferro- or ferrimagnetic crystals. Initially, the practical interest in the chiral compounds was based on their magneto-optical properties and a possibility to use the Faraday effect in the optically transparent magnets.[14] Despite the extensive experimental research, no effect of chirality on the magnetic properties of solids has been experimentally proven until now. The main reason for the discrepancy between theoretical predictions and experimental data consists in the generally inappropriate experimental techniques used for the analysis of the magnetic properties. In particular, a superconducting quantum interference device (SQUID) magnetometer is routinely used for the investigation of synthesized materials. While this method allows determining of the total magnetic moment M of the sample, it integrates all magnetic contributions and, thus, masks any direct information about the spin-wave excitations. The invariant behavior of the magnetic moment to the inversion of the coordinate axis is one of the fundamental properties of magnetism. However, this excludes the possibility of observing the influence of spin chirality on the magnetic moment in any sample. As a result, a very popular viewpoint that the magnetic properties of solids are insensitive to the chiral contribution has been established.

This paper aims to challenge the opinion mentioned above. It is clear that spin chirality can influence spin-wave phenomena such as the generation, annihilation, and propagation of both spin waves and spin solitons if these excitations exist in a magneto-ordered phase of the material. Differences between the EPR spectra in racemic and chiral crystals were previously reported even for paramagnetic phases.[16,17] Also, in such crystals, one can expect additional types of spin excitations to be prohibited in central symmetric nonchiral crystals. For example, three-dimensional (3D) solitons of spin density were predicted in molecular chiral yellow needle (YN) magnets[8] and some indirect experimental confirmations were obtained. Previously, we reported observation of magnetic resonant spectra corresponding to the spin-soliton resonance excited by the microwave field in chiral ferrimagnets.[18] In the past, spin solitons were observed in thin ferromagnetic films only. In this work, we present the results of a systematic investigation of the collective spin excitations in chiral and racemic molecular based crystals,

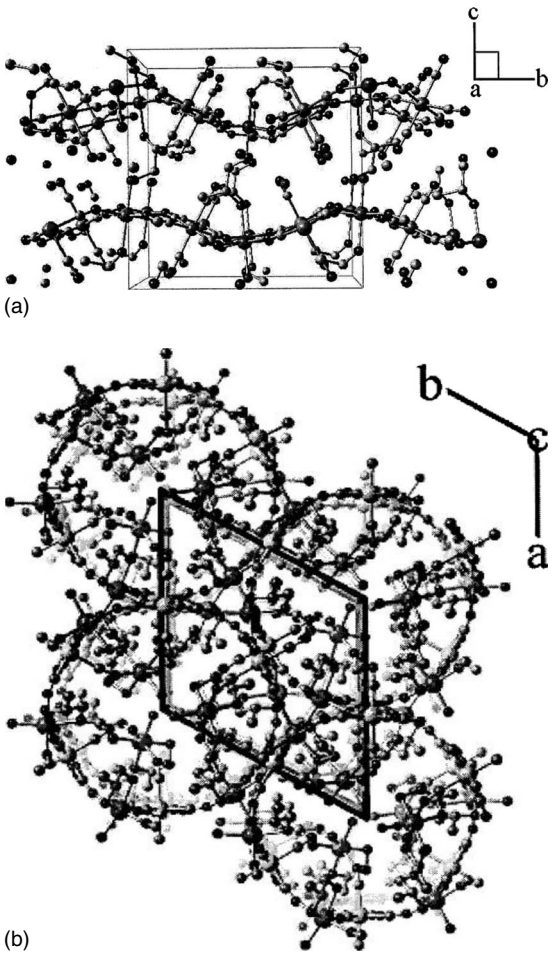

FIG. 1. Atomic structure of the chiral crystals: (a) green needle (GN), along the *a* axis; (b) yellow needle (YN), along the *c* axis.

which are distinguished by their crystal structure and the dimensionality of the exchange interaction. In layered two-dimensional (2D) green needle (GN) crystals, we observed two-dimensional spin ordering in molecular layers formed by alternative Mn^{2+} and Cr^{3+} ions [Fig. 1(a)]. Evidence of two-dimensional magnetic ordering in GN crystals was also obtained in Ref. 19, wherein we reported the main magnetic parameters of the ferromagnetic state, e.g., the anisotropy field, H_a=2500 Oe and the Curie temperature, T_c=37 K. The spin dynamics in ferrimagnetic YN crystals was studied in Ref. 20, wherein the main parameters of a 3D ferrimagnetic state in YN crystals were found (the Curie temperature, T_c=53 K, and the easy magnetization direction is oriented along the *c* axis).

The aims of the current work are the investigation of different kinds of resonances and the influence of chirality on magnetic resonant spectra, the observation of spin-wave phenomena, as well as the comparison and analysis of the ESR spectra in chiral and racemic crystals with 2D and 3D magnetic spin orderings in GN and YN crystals, respectively.

II. EXPERIMENT

Dielectric, optically transparent $\{Mn[(R/S)\text{-}pn]\}_2\{Mn[(R/S)\text{-}pn]_2(H_2O)\}[Cr(CN)_6]$ single crystals have been synthesized as plate elongated rectangular needles of a yellow color (YNs). As prepared $Cr(CN)_6[Mn(S)\text{-}pn H\text{-}(H_2O)]H_2O$ single crystals have been prepared as GNs. The studied crystals have a size of $\sim 2\times 0.5\times 0.05$ mm^3, which was determined by using an optical microscope. The chemical synthesis and crystal growth of these crystals were reported in detail in Ref. 13. The x-ray analysis of the hexagonal YN crystals reveals a three-dimensional chiral network [Fig. 1(b)]. Four cyanide groups of $[Cr(CN)_6]^{3+}$ ions are coordinated by Mn^{2+} ions forming helicoidally bimetallic loops with their axes parallel to the *c* axis, lying along the longest edge of the needle shaped crystal. The atomic structure of GN is shown in Fig. 1(a). In the GN crystals, the *c* axis was also directed parallel to the longest edge of the needle shaped crystal. In our experiments, we used both the chiral and racemic GN crystals. The racemic GN crystals have a crystal structure with alternating "left" and "right" ligands. For this reason, any possible chiral effects are mediated to zero. Thus, three types of crystals have been studied in our work: chiral and racemic GN crystals and chiral YN ones. No racemic YN crystals have been investigated.

A Bruker ESR 500 electron spin resonance spectrometer with an x-band resonator (microwave frequency is $\nu \sim 9.5$ GHz) was equipped with a rectangular microwave cavity H_{102}. The modulation frequency was 100 kHz in all experiments. The quality of the resonator Q=12000–13000 at T=4 K was stable during the spectra recording and the resonance detection. The measured signal intensity I was proportional to the first derivation of the imaginary part of the magnetic susceptibility of the crystal, $I \sim d\chi/dH$. The temperature was varied in the range of T=4–290 K by using an ESR 900 Oxford instruments cryostat. In the most interesting temperature range of T=4–70 K, the temperature was stable with an accuracy of $\pm 5\times 10^{-3}$ K. The microwave power was varied in the range of 10^{-6}–10^{-1} W, and it was 10^{-4} W in most of the experiments. Special precautions were undertaken to control the microwave frequency, which was automatically stabilized and was stable during the spectral recording within 10^{-6} of the spectrometer frequency. The YN crystal was sealed in a quartz tube filled with argon. The paramagnetic a'-diphenyl-β-picryl hydrazyl sample was used as a reference sample for the calibration of the *g* factor.

A microwave field can generally excite the magnetoelastic resonance modes (Walker modes)[21] in ferromagnets. To prevent the formation of such modes and their mixing with the resonant lines of other types, we studied YN crystals of different shapes. Two pieces of YN crystal of the same thickness but different lengths and shapes were chosen for comparison of their spectra at the same rest conditions. These pieces were produced by breaking the single needle crystal. For that reason, the thicknesses of the pieces were the same. Since the volumes of these pieces differed by about two times, the spectra amplitudes were normalized on the same value. It was found that the ESR spectrum did not depend on the shape of the YN crystals (Fig. 2). The small discrepancy between these two spectra could be explained by a possible deviation of the orientations of the samples within 5°. Thus, the magnetoelastic mode contribution is negligibly small in comparison to the observed resonance spectra. Other evi-

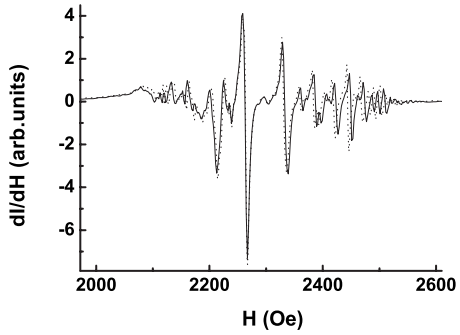

FIG. 2. Spectra of the electron spin resonance of the chiral YN crystals at 9 K. The dc magnetic field of the ESR spectrometer is directed along the easy magnetization c axis. The solid line is a spectrum of the rectangular YN crystal of 1 mm length and the dotted line is a spectrum of the YN crystal of 0.3 mm length with an irregular shape at the ends. The spectra are normalized to the same amplitude.

dence of this fact will be presented in Sec. III. As it will be shown below, the influence of chirality on the resonant line independently sequenced on the shape of the crystals is strong evidence of the spectral sensitivity to the molecular structure of the crystals.

III. EXPERIMENTAL RESULTS AND DISCUSSION

A. Spectra of the electron spin resonance in chiral two-dimensional and three-dimensional crystals

Single Lorentz lines have been observed in the paramagnetic state of both the GN and the YN crystals at temperatures higher than 37 K (for the GN crystals) and 53 K (for the YN crystals). The temperature and angular dependences of these lines were studied in detail in Refs. 19 and 20. In this paper, the main attention will be focused on the investigation of the collective spin excitations at temperatures below the Curie point.

At the temperature $T=4$ K (and other temperatures below $T_c=53$ K), a complex magnetic resonance spectrum has been observed in the YN crystals (Fig. 3). This spectrum can be described as two line sequences: (i) **1a**,**2a**,**3a**… are peaks whose amplitudes decrease as the magnetic field decreases ("left-hand" sequence) and (ii) **1b**,**2b**,**3b**… are peaks whose amplitudes decrease as the magnetic field increases ("right-hand" sequence). The maximal number of lines in these sequences reaches 30–40 (the first four lines are labeled in Fig. 3). Each peak has its own satellites and could be described by a fine structure. We will not consider this fine structure here and will focus our attention on the main strongest peaks.

In the GN crystals, the spectrum of the electron spin resonance contains two peak sequences located in the low- and high-field parts of the spectrum. In both sequences, the line amplitude reduces as the magnetic field increases (Fig. 4). The ESR spectra of the chiral and racemic GN crystals are strongly different [see Figs. 4(a) and 4(b) for comparison]. The right-hand sequence in the chiral GN crystals contains peaks, whose linewidth H_{pp} and the interval between peaks,

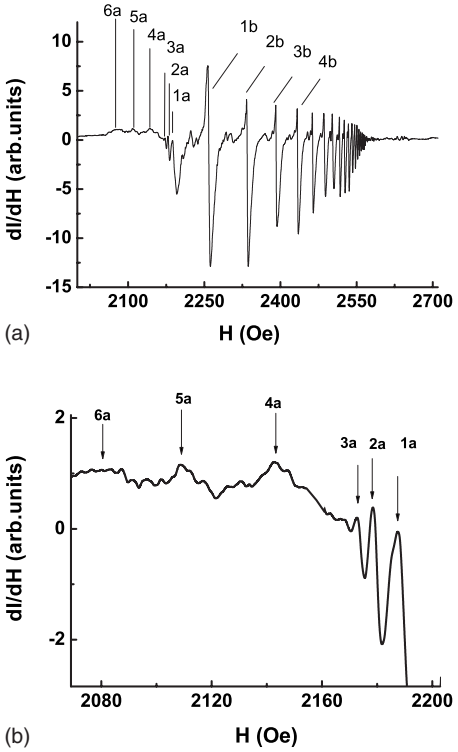

FIG. 3. Spectrum of the electron spin resonance of the chiral YN crystals at 4 K. The dc magnetic field of the ESR spectrometer is directed along the easy magnetization c axis. (a) is a full spectrum and (b) is its fragment with left-handed sequence.

$\Delta H=H_{\mathrm{res},i+1}-H_{\mathrm{res},i}$, decrease as the magnetic field increases [Fig. 4(a)]. In the racemic GN crystals, both the H_{pp} and the ΔH values in the right-hand sequence increase as the magnetic field increases [Fig. 4(b)].

The left-hand decaying sequences have been observed only in the GN crystals when the static magnetic field is oriented along the c axis (Fig. 5). These left-hand sequences are identical to each other in the chiral [Fig. 5(a)] and the racemic [Fig. 5(b)] GN samples and are very similar to the left-hand sequences in the YN crystals.

Separation of the peak sequences for the left-hand and right-hand decreasing ones was possible for the determined orientation of the magnetic field of the spectrometer. However, in general, the overlapping of the resonances and the intermixture of the left-hand and right-hand sequences have been observed for arbitrary orientations of the field. Comparison and analysis of these spectra are very complicated. However, as it will be shown below, a comparison of the magnetic susceptibilities corresponding to the integral amplitude of each resonance enables us to distinguish the peaks even in such an intricate situation.

B. Spin-wave resonance

The good reproducibility of the spectrum in the samples of different shapes and sizes, as well as a large number of resonant peaks, rules out an influence of the magnetoelastic modes as a possible reason of the observed effects. Therefore, it is necessary to consider other types of collective spin

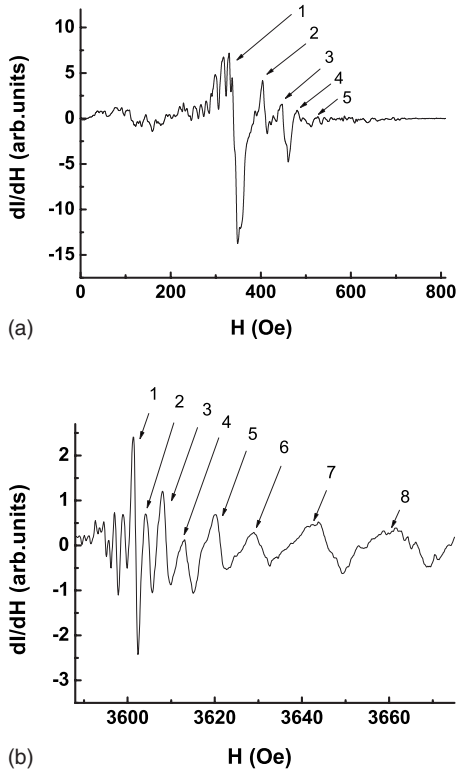

FIG. 4. Spectra of the electron spin resonance recorded at 4 K in (a) the chiral GN crystal, with the magnetic field oriented at 30° to the *a* axis; and (b) the racemic GN crystal, with the magnetic field oriented along *a* axis.

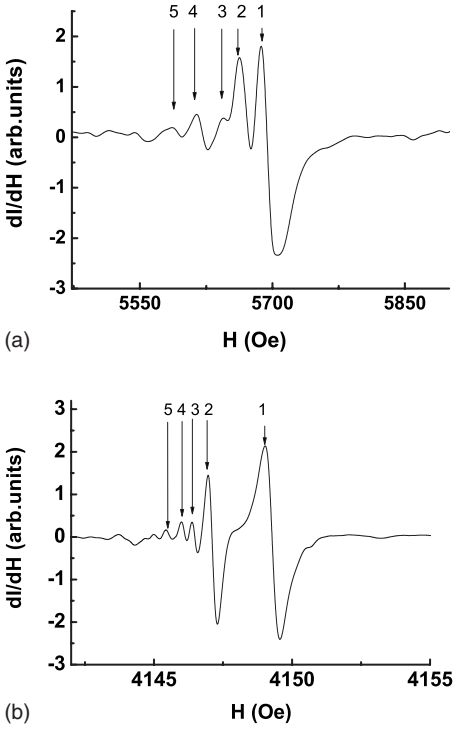

FIG. 5. Spectra of the electron spin resonance recorded at 4 K, the static magnetic field is oriented along the *c* axis: (a) chiral GN crystal; (b) racemic GN crystal.

excitations in magnetically ordered solids. One of the possible types of resonances leading to the multipeak spectra is the spin-wave resonance (SWR).[1] Usually, this kind of resonance arises in thin films with a thickness of ~10–100 nm. Standing spin waves excited by a microwave field usually have the wavelength compatible with the film thickness. One of the conditions of the SWR observation in homogeneous films is a linear dependence of the resonant field H_{res} on the square of the resonant peak number n

$$H_{\mathrm{res}} = H_0 - D(\pi n/d)^2, \tag{1}$$

where H_0 is the resonant field of the homogeneous mode, which corresponds to the ferromagnetic resonance, D is the exchange stiffness constant, and d is the film thickness. This relation [Eq. (1)] between H_{res} and n can be observed for different conditions of the spin pinning to the film surface. Standing spin waves can be excited even in the case wherein the spin direction is unpinned at one interface and pinned at the other by the magnetic anisotropy.[22] This case of partly pinned spins is the most probably realized in our crystals with a large thickness ($d \sim 20\,000$ nm). One of the manifestations of the SWR is the decrease in the peak amplitudes with the magnetic field.[4] To the best of our knowledge, there are no such boundary conditions that could provide the opposite direction of the peak amplitude decrease. Therefore, here, we use only the left-hand sequences of the resonances to check the SWR assumption. In the chiral YN crystals, the $H_{\mathrm{res}}(n^2)$ dependence is linear with a high accuracy (95%–99%) at all temperatures below T_c and magnetic field orientations [Fig. 6(a)]. The right-hand part of the spectrum (where the amplitude of resonances decreases in the direction

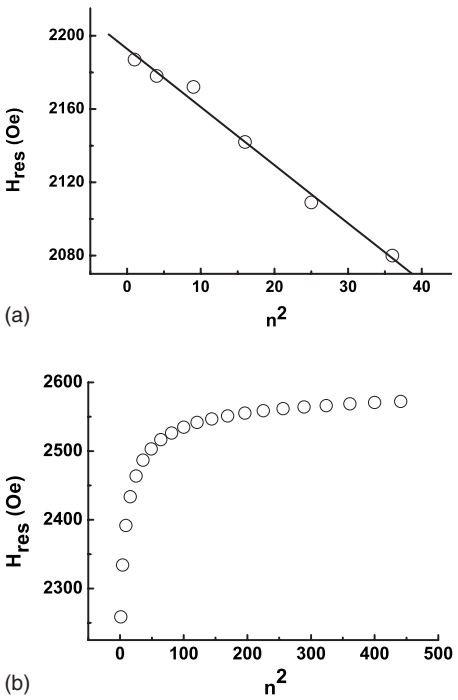

FIG. 6. Dependence of the resonant field H_{res} on the square of the wave mode number, n^2 in the chiral YN crystal: (a) for modes of the left-hand sequence in Fig. 3; (b) for modes of the right-hand sequence in Fig. 3.

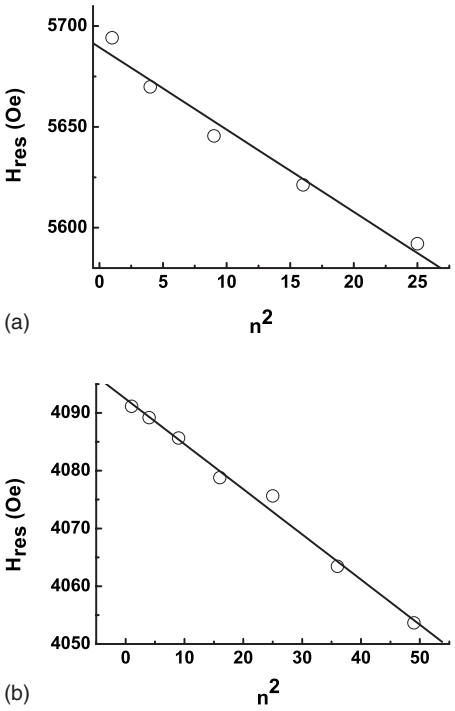

FIG. 7. Dependence of the resonant field H_{res} on the square of the wave mode number n^2 measured at 4 K, the static magnetic field is oriented along the c axis: (a) chiral GN crystal; (b) racemic GN crystal.

of the high magnetic field) does not obey the condition in Eq. (1), i.e., the dependence $H_{res}(n^2)$ is not linear [Fig. 6(b)]. This behavior will be considered later within the frame of the different spin resonant phenomena. In both the chiral and the racemic GN crystals, $H_{res}(n^2)$ dependences are linear [see Figs. 7(a) and 7(b)], respectively.

The exchange stiffness constant $D=2A_{eff}/M$, which is extracted from Eq. (1), and the corresponding slope of the $H_{res}(n^2)$ dependence give us an opportunity to calculate the exchange interaction constant A_{eff}. The saturation magnetization of the sample, $M=1500$ emu/mol, is known from previous SQUID measurements for both the YN and the GN crystals.[8] Thus, the following expression for the exchange interaction constant can be obtained for two different peaks i and j in the left side of the resonant spectrum:

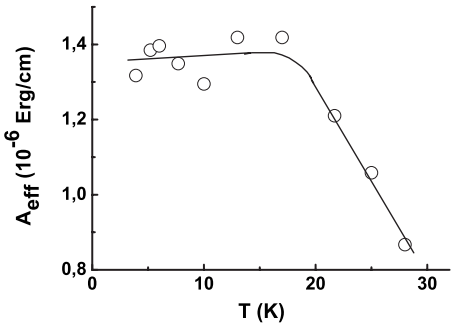

FIG. 8. Temperature dependence of the effective exchange interaction, A_{eff}, calculated for the racemic GN crystals from the $H_{res}(n^2)$ dependence recorded at 4 K. The magnetic field is oriented along the c axis.

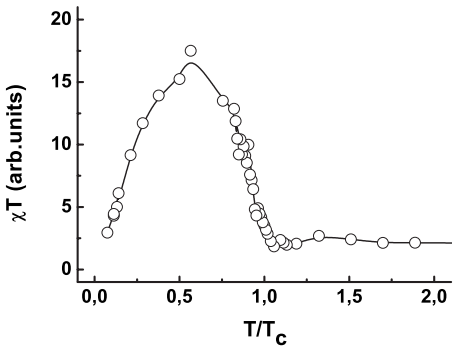

FIG. 9. Temperature dependence of the magnetic susceptibility χ multiplied by the temperature T in the chiral YN crystals. The magnetic field is orientated along the c axis. The magnetic susceptibility χ was calculated by double integration of the ESR spectrum.

$$A_{\text{eff}} = \frac{\langle M \rangle}{2} \frac{H_{\text{res},i} - H_{\text{res},j}}{n_j^2 - n_i^2} \left(\frac{d}{\pi} \right)^2, \tag{2}$$

where $d=20\,000$ nm. The temperature dependence of the exchange interaction constant $A_{eff}(T)$ is shown in Fig. 8 for the GN crystals. In the GN crystals, the temperature dependence $A_{eff}(T)$ indicates a sharp fall of the exchange interaction at temperatures above 20 K (Fig. 8). Close to the Curie temperature ($T_c=37$ K), the exchange interaction constant decreases. We have found a good correlation between the temperature dependencies of the exchange interaction constant and the magnetic susceptibility (Fig. 9).

Figure 10 demonstrates the orientation dependence of the exchange interaction constant $A_{eff}(\Theta)$, where Θ is the angle between the magnetic field and the c axis of the crystal. The angular dependence has been measured by the rotation of the sample in the ac plane of the crystal. The angular dependence $A_{eff}(\Theta)$ demonstrates that the maximal exchange interaction occurs when the magnetic field is oriented along the easy a axis. This fact indicates that the exchange interaction within the molecular layer is stronger than the interlayer interaction and agrees well with earlier results,[17] wherein the same conclusion was drawn from the analysis of a single

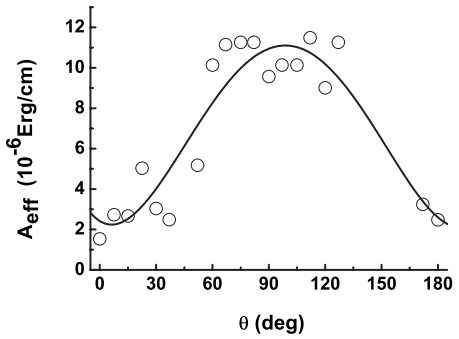

FIG. 10. Angular dependence of the effective exchange interaction, A_{eff}, calculated for the racemic GN crystals from the $H_{res}(n^2)$ dependence recorded at 4 K. The magnetic field is parallel to the ac plane during the rotation of the sample around the b axis. The angle $\theta=0$ corresponds to the orientation of the magnetic field along the c axis.

Lorentzian line in the paramagnetic state of the GN crystals.

Similar values of the exchange interaction $A_{\text{eff}} = 10^{-5} - 10^{-6}$ erg/cm have been determined for the YN crystals. These values are 1–2 orders of magnitude smaller than the correspondent parameter in metallic magnetic films.[4] This can be explained by the fact that metal-organic GN and YN compounds have a much lower spin-density than metals and the exchange interaction in our crystals indirectly propagates through CN bonds.

C. Spin-soliton resonance

In this paragraph, we discuss the right-hand peak sequences observed in both the YN and the GN crystals. Figure 6(b) shows that the right-hand sequences do not satisfy the SWR condition and, hence, correspond to other types of collective spin resonant phenomena. The right part of the ESR spectrum in the YN single crystal contains a consequence of the resonant lines whose amplitudes decrease with the increasing magnetic field at 4 K in the x-band spectrometer. Similar spectra have been observed at higher temperatures up to the Curie point $T_c = 53$ K (Fig. 3). The shape of these spectra does not depend on the sweeping rate of the magnetic field, which is varied depending on the recording, $t_R = 40 - 640$ ms. The spectrum appeared as a sequence of 20–30 Lorentzian lines and it was well reproducible for the same or different samples. The large amount of resonance lines observed in our experiments rules out the possibility of ferrimagnetic resonance, although this type of resonance would be expected in the GN and the YN crystals.

It was shown that the competition between the two types of interactions (anisotropic and DM exchange interactions) in noncentral symmetric crystals leads to a chiral spin arrangement.[8] Both isotropic and DM exchange interactions, as well as the Zeeman energy of spins, give contributions to the spin Hamiltonian

$$H = -J\sum_n \mathbf{S}_n \cdot \mathbf{S}_{n+1} - \mathbf{D} \cdot \sum_n \mathbf{S}_n \times \mathbf{S}_{n+1} - 2\mu_B \mathbf{H} \cdot \sum_n \mathbf{S}_n$$

$$= -S^2 \tilde{J} \sum_n \cos(\phi_{n+1} - \phi_n - \alpha) - 2\mu_B S \sum_n \cos\,\phi_n, \qquad (3)$$

where ϕ_n represents the pitch angle of the electron spin $\mathbf{S}$ on the nth site along the chiral axis, J is the isotropic exchange integral, $\mathbf{D}$ is the Dzyaloshinskii–Moriya exchange integral, $\tilde{J} = \sqrt{J^2 + D^2}$, $\alpha = \tan^{-1}(D/J)$ is the fixing pitch angle, $\mathbf{H}$ is the magnetic field, and μ_B is the Bohr magneton. The above Hamiltonian leads to the effective Ginzburg–Laudau free energy functional

$$F_{m,\phi} = \frac{\tilde{J}m^2}{L} \int \left[\frac{1}{2} \left(\frac{d\phi}{dz} \right)^2 - \alpha \frac{d\phi}{dz} - \beta \cos\,\phi \right] dz, \qquad (4)$$

where the thermal average of the magnetic moment is treated as a continuous variable depending on the z position along the chiral axis and is written as $\mathbf{M} = m(T)[\cos\,\phi(z), \sin\,\phi(z)]$. The energy minimization gives an equilibrium orientation of the spins, whose space distribution obeys the Sin–Gordon equation corresponding to the spin soliton for the determined relation between the D and J parameters. The soliton energy is proportional to the spatial period of the chiral soliton lattice, L, controlled by the local magnetic field H according to the equation $L = 4k[K(k)]\sqrt{\tilde{J}S/H}$, where S is the effective spin value, H is the local magnetic field, which is the sum of the external and internal fields, k $(0 < k < 1)$ is the elliptic modulus, and $K(k)$ is the elliptic integral depending on the spin orientation and the anisotropy field.[8] In the present experiments, the strength of the applied magnetic field was much smaller than the critical field strength H_c corresponding to the incommensurate-to-commensurate phase transition and was defined as

$$m(T, H_c) = \frac{H_c}{\tilde{J}} \left(\frac{4}{\pi\alpha} \right)^2. \qquad (5)$$

From this equation, we see that the critical field $H_c \sim 50$ kOe is comparable to that of $\tilde{J}$ that is clearly much larger than the field strength $H \sim 1$ kOe used in our experiments. Thus, for small magnetic fields, i.e., $H \ll H_c$, we can imply that the elliptic function $K(k)$ is not singular and almost constant. Therefore, $L \sim 1/\sqrt{H}$ and, thus, the energy associated with the soliton lattice formation is also proportional to $1/\sqrt{H}$. Now, if we assume coincidence of a microwave energy quanta $h\nu = \mu g H_{\text{res}}$ with the energy of a soliton excitation, we should expect that the interval between neighboring resonant maxima i and $(i+1)$, $\Delta H = H_{\text{res},i+1} - H_{\text{res},i}$, will be inversely proportional to the square root of the magnetic field strength $\Delta H \sim 1/H^{1/2}$.

The external magnetic field applied in the plane of the spiral creates a competition between the spiral order with the ground state wave vector q^* and the homogeneous magnetization along the field direction, leading to the magnetic order described by a soliton lattice (SL) with a wave vector $q < q^*$; i.e., the lattice Bloch wave vector q^* is not a good quantum operator in the SL state.[12] Indeed, for fields below the critical magnetic field H_c, corresponding to a nearly uniform spin polarization along the field direction, the spiral state is driven by the field to a SL state in which the magnetization orientation periodically slips from the field-direction orientation. At $H = H_c$, the uniform state has the same energy as the state that accommodates a single soliton. For $H < H_c$ the magnetic state can be described as a soliton lattice with a period L. The associated wave vector $q = 2\pi/L$ varies from $q = 0$ at $H = H_c$ to $q = q^*$ at $H = 0$. In the latter limit, the SL state approaches the spiral magnetic order of the ground state. The total phase change along the sample is given by qL_S, where L_S is the length of the sample. Therefore, the condition of resonant generation of the soliton lattice is given by $qL_S = 2\pi n$ (n is an integer), or $L_S = n\,L$.

Figure 11 presents a vector model of the predicted spin excitations in the system. Under the action of the magnetic field, a kink with the length $L \sim (JS/H)^{1/2}$ arises in a homogeneous spin structure. One can expect the generation of solitons with different lengths in resonant conditions if the energy of the microwave quanta will coincide with the energy of the kink formation, $E \sim L \sim (JS/H)^{1/2}$ [Fig. 11(b)]. In this case, the condition of a spin-soliton resonance can be written as

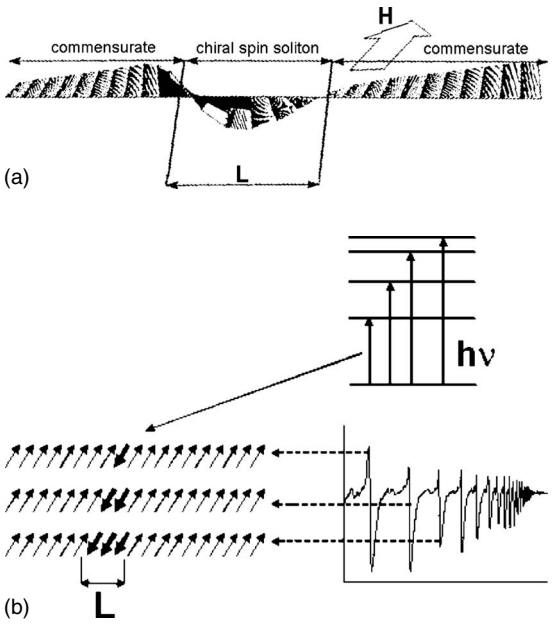

FIG. 11. Schematics of (a) the distribution of the spin density corresponding to a spin soliton in a crystal (L is the length of the soliton) and (b) the correlation between the SW resonant peaks, energy levels, and geometrical parameters (length L) in a soliton.

$$h\nu = \mu_B \mu_0 g H_{\text{ferro}} + k/H_{\text{res}}^{1/2}, \tag{6}$$

where $k \sim 1$ is the field-independent coefficient, μ_0 is the magnetic constant, and $g \sim 2$ is the g factor. One can expect decreasing in the resonant amplitudes with the magnetic field increase, since the probability of excitation of long solitons is lower than short ones. In the experiment, it might be observed as a sequence of decreasing resonant peaks, as the kink length also discretely changes [Fig. 11(b)]. The field interval between the nearest neighbor peaks should become shorter if the magnetic field increases within the frame of the spin-soliton model, as the energy difference necessary for the creation of the 99th and 100th solitons should be smaller than the energy difference between the first and second ones.

In order to prove the above model, we identified intervals between neighboring resonant peaks and plotted them as a function of the magnetic field, whose value was chosen as the center of neighboring i and $(i+1)$ resonant fields, $(H_{\text{res},i+1}+H_{\text{res},i})/2$. The experimental dependence ΔH vs $(1/H^{1/2})$ is a straight line if the magnetic field is oriented along the easy magnetization axis of the chiral YN (Fig. 12) and the chiral [Fig. 13(a)] GN crystals. This observation allows us to identify the right peak sequences as spin-soliton resonances in the chiral crystals.

In the racemic GN crystals, the slope of the ΔH vs $(1/H^{1/2})$ dependence is negative in contrast to the chiral crystals [Fig. 13(b)]. If we are to assume that the spin-soliton resonance can be excited in racemic crystals as well, we obtain a contradiction with the model described above. This model predicts a decrease in the interval between the neighboring peaks in contrast to our experimental data. Thus, in the racemic crystals, we have observed some additional spin resonance. Further experimental investigations are required

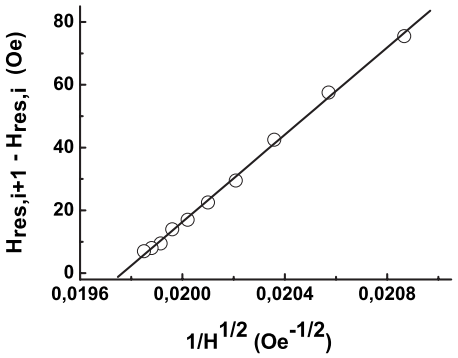

FIG. 12. Dependence of the interval between the neighbor resonant maxima, $H_{\text{res},i+1}-H_{\text{res},i}$, on the square root of the magnetic field strength in the right-hand sequence in Fig. 3 in the chiral YN crystal at 4 K.

in order to clarify the nature of this type of spin resonances in racemic crystals.

Generally, soliton phenomena are characterized by nonlinearity and a threshold value of the magnetic field controlling the soliton generation.[3] In our experiments, we have found such a threshold value by using the rotation of the crystal in the ESR spectrometer (only the projection of the static magnetic field on the c-axis direction was considered). Figure 14 shows the ΔH vs $(1/H^{1/2})$ dependences measured at different angles between the c axis of the YN crystal and the magnetic field. As the angle increases, the slope of the correspondent

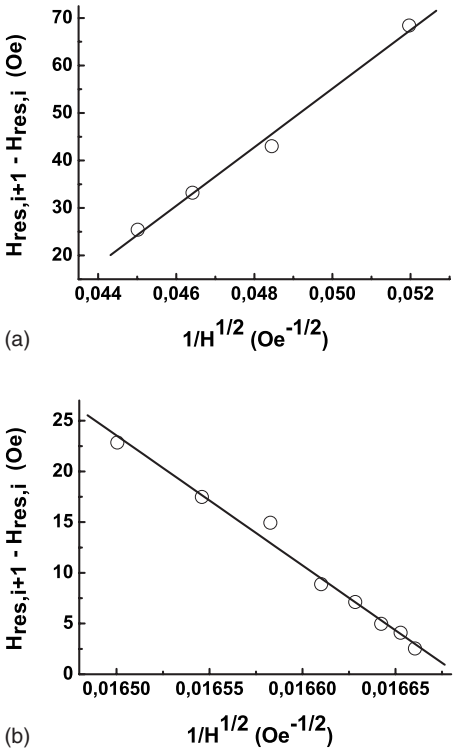

FIG. 13. Dependence of the interval between the neighbor resonant peaks, $H_{\text{res},i+1}-H_{\text{res},i}$, on the square root of the magnetic field strength in (a) the chiral GN crystals, in which the dc magnetic field is oriented at 30° to the a axis, and (b) the racemic GN crystals, in which the dc magnetic field is oriented along the a axis.

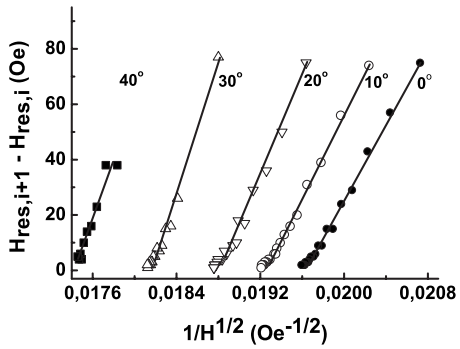

FIG. 14. Dependences of the interval between the neighbor resonant maxima, $H_{res,i+1}-H_{res,i}$, on the square root of the magnetic field strength for the resonant peaks of the right-hand sequence in Fig. 3 in the YN chiral crystals at 4 K at different angles between the dc magnetic field and the easy magnetization c axis.

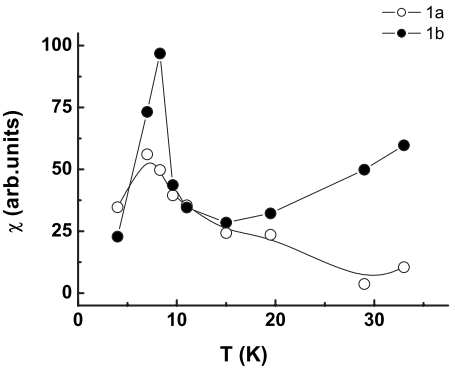

FIG. 15. Temperature dependences of the magnetic susceptibilities, calculated by double integration of lines 1a and 1b in the left-hand and right-hand peak sequences in the YN chiral crystals. The dc magnetic field is oriented along the c axis of the crystal.

dependence also increases. In the narrow angle range, 45°–50°, the right-hand sequence disappears and only the left-hand sequence is observed (Fig. 5). The obtained threshold value of 1500 Oe is a typical fingertip of the nonlinear spin-wave phenomena.

The temperature dependences of the ESR parameters for the left-hand and right-hand peak sequences are different. Figure 15 shows the temperature dependences of the magnetic susceptibilities for lines 1a and 1b (Fig. 3). The susceptibility values have been calculated by multiplication of the square of the linewidths on the line amplitude at each temperature. A difference between the temperature dependences has been observed for peaks of the left-hand and right-hand sequences. However, a comparison of the peaks within the same sequence shows no differences. This fact confirms the existence of additional collective spin-wave phenomena instead of a spin-wave resonance. For an arbitrary orientation of the magnetic field, SWR and SSR lines can be distinguished by temperature dependences of the magnetic susceptibilities.

It might be suggested that the difference between the resonant spectra of the GN and YN crystals originates in the nature of the helical ground state in these materials. The YN compound belongs to a class of helimagnets with a significant finite-period helical ground state ordering.[8] The pitch of the spin screw is on the order of ten or hundred lattice constants. In this case, magnetic ions are located in a line along with the spiral that is common for magnetic crystals with the space group PN_1. The magnetic field perpendicular to the spiral axis generates the sequence of SL states with an increasing period L in accordance with the "quantization" condition $L_S=nL$. In contrast to the YN crystal, the GN crystal has a long-period helical ground state that is due to the Dzyaloshinskii instability and the chiral spin ordering occurs along a crystallographic axis. The zero-field wave vector $q^*=\tan^{-1}(D/J)$ is relatively small and the corresponding pitch $2\pi/q^*$ becomes quite long, having the same order as the sample length. In this case, a helical ground state most probably accommodates a single soliton that excludes the SL formation by the external field. Thus, a few reasons exist why we cannot describe the right sequence within the frame of the theory magnetostatic modes:

(i) Independence of the resonant spectrum on the shape and length of the crystals at the constant thickness.

(ii) Effect of the chirality on the sequence of resonant maxima. In the case of magnetostatic modes, there should not be any difference between the racemic and chiral crystals.

(iii) Difference in the temperature dependencies of the right and left series of the peaks.

(iv) Existence of the threshold value of the projection of the magnetic field on the crystal axis at which a right sequence disappeared.

IV. CONCLUSIONS

Two different types of electron spin resonance, namely the spin-wave and the spin-soliton resonances, are found in YN and GN chiral crystals. The threshold value of the magnetic field projection on the easy magnetization axis is observed. This projection corresponds to a minimal magnetic field of ~1500 Oe, which is sufficient for a soliton excitation by the microwave magnetic field. It has been shown that in racemic crystals, the spin-soliton resonance does not exist at the same experimental conditions as in chiral crystals. Thus, in this work, the first direct evidence of the chirality influence on the type of collective spin excitations initiated by the microwave magnetic field was received. The analysis of spin-wave resonant spectra allows us to determine the effective exchange interaction, 10^{-5}–10^{-6} erg/cm, and its dependence on the sample orientation and temperature.

ACKNOWLEDGMENTS

The authors thank the Institute for Molecular Science (Japan) for ESR spectrometer and Japanese Society for the Promotion of Science for the financial support (project P 05388) and V. Berdinskii for fruitful discussions.

[1] A. I. Ahiezer, A. I. Bariyahtar, and S. V. Peletminskii, *Spin Waves* (Nauka, Moscow, 1967), p. 368.
[2] N. M. Salanskii and M. Sh. Eruhimov, *Physical Properties and Application of Thin Films* (Nauka, Novosibirsk, 1975), p. 222.
[3] A. M. Kosevich, B. A. Ivanov, and A. S. Kovalev, Phys. Rep. **194**, 117 (1990).
[4] A. G. Gurevich and G. A. Melkov, *Magnetic Vibrations and Waves* (Nauka, Moscow, 1994), p. 464.
[5] R. Skomski, J. Phys.: Condens. Matter **15**, 841 (2003).
[6] M. I. Chipara, R. Skomski, and D. J. Sellmyer, J. Magn. Magn. Mater. **249**, 246 (2002).
[7] S. A. Zvyagin, A. K. Kolezhuk, J. Krzystek, and R. Feyerherm, Phys. Rev. Lett. **95**, 017207 (2005).
[8] J. Kishine, K. Inoue, and Y. Yoshida, Prog. Theor. Phys. **159**, 82 (2005).
[9] B. Roessli, J. Schefer, G. A. Petrakovskii, B. Ouladdiaf, M. Boehm, U. Staub, A. Vorotinov, and L. Bezmaternikh, Phys. Rev. Lett. **86**, 1885 (2001).
[10] A. Zheludev, S. Maslov, G. Shirane, Y. Sasago, N. Koide, and K. Uchinokura, Phys. Rev. B **57**, 2968 (1998).
[11] A. Beghidja, G. Rogez, P. Rabu, R. Welter, and M. Drillon, J. Mater. Chem. **16**, 2715 (2006).
[12] K. Inoue, H. Imai, P. S. Ghalsasi, K. Kikuchi, M. Ohba, H. Okawa, and J. V. Yakhmi, Angew. Chem. **113**, 4372 (2001).
[13] K. Inoue, K. Kikuchi, M. Ohba, and H. Okawa, Angew. Chem., Int. Ed. **42**, 4810 (2003).
[14] E. Coronado, J. R. Galan-Mascaros, C. J. Gomez-Garcia, and A. Murcia-Martinez, Chem.-Eur. J. **12**, 3484 (2006).
[15] K. Ohishi, W. Higemoto, A. Koda, S. R. Saha, R. Kadono, K. Inoue, and H. Higashikawa, J. Phys. Soc. Jpn. **1**, 1 (2006).
[16] V. K. Khlestkin, Y. I. Glasachev, A. I. Kokorin, and R. G. Kostyanovsky, Mendeleev Commun. **14**, 318 (2004).
[17] T. Fujita, S. Mitsudo, M. Toda, T. Idehara, M. Chiba, K. Inoue, and M. Motokawa, Low Temperature Physics: 24th International Conference on Low Temperature Physics, Orlando, Florida, USA, 2005, edited by Y. Takano, S. P. Hershfield, S. O. Hill *et al.* (2006), Paper No. CP850, p. 1055.
[18] R. B. Morgunov, V. L. Berdinskii, M. V. Kirman, K. Inoue, J. Kishine, Y. Yoshida, and Y. Tanimoto, Pis'ma Zh. Eksp. Teor. Fiz. **84**, 524 (2006) [JETP Lett. **84**, 446 (2006)].
[19] I. V. Blokhin, A. S. Markosyan, R. B. Morgunov, K. Inoue, Y. Tanimoto, and Y. Yoshida, Phys. Solid State **47**, 2016 (2005).
[20] R. B. Morgunov, M. V. Kirman, K. Inoue, Y. Yoshida, and Y. Tanimoto, Chem. Phys. **26**, 84 (2007).
[21] L. R. Walker, Phys. Rev. **105**, 390 (1957).
[22] A. Layadi, J.-W. Lee, and J. O. Artman, J. Appl. Phys. **63**, 3808 (1988).